

Publication status: This preprint has not been published elsewhere.

# Linking 3D Perinereis burrows with physicochemical factors on a tidal flat (Pearl River Delta (PRD), China)

Yuanyuan Wang, Zhen Zhang, Miao Miao, Manzhi Yang, Guocheng Zhang

<https://doi.org/10.1590/2675-2824074.2502>

Submitted on: 2026-06-05

Posted on: 2026-06-12 (version 1)

(YYYY-MM-DD)

## Linking 3D *Perinereis* burrows with physicochemical factors on a tidal flat (Pearl River Delta (PRD), China)

WANG Yuanyuan<sup>1,2\*</sup>, ZHANG Zhen<sup>1</sup>, MIAO Miao<sup>1</sup>, YANG Manzhi<sup>1</sup>, ZHANG Guocheng<sup>1,2</sup>

Y.W.:  <https://orcid.org/0000-0002-8470-4456>

Z.Z.:  <https://orcid.org/0009-0004-8880-9724>

M.M.:  <https://orcid.org/0009-0008-5399-1246>

Y.M.:  <https://orcid.org/0009-0002-7576-6951>

G.Z.:  <https://orcid.org/0000-0002-3021-7353>

1 Institute of Resource and Environment, Henan Polytechnic University, Jiaozuo 454003, Henan, China

2 Henan International Joint Research Laboratory for Biogenic Traces and Sedimentary Minerals, Jiaozuo 454003, Henan, China

\* Corresponding author: [yyw@hpu.edu.cn](mailto:yyw@hpu.edu.cn)

### Abstract

This study employed a comprehensive approach involving field sampling, grain-size analysis, physicochemical measurements, CT scanning and three-dimensional reconstruction in order to investigate the intertidal flats of the Pearl River Delta (PRD). As *Perinereis* is an important group of bioindicators in relation to environmental factors, sedimentological and ichnological analyses were conducted at 6 out of 63 stations. These analyses aimed to clarify the composition and distribution characteristics of *Perinereis* traces, reveal their response relationships with physicochemical factors including sediment grain size, salinity, turbidity and total organic carbon (TOC) content, and further illustrate their environmental significance. The results showed that: (1) *Perinereis* traces are predominantly composed of grazing and dwelling burrows. These burrows display diverse morphologies, including simple cylindrical, Y-shaped, U-shaped and complex branching networks. Some branches exhibit swellings at junctions. (2) Salinity has a significant influence on the burrow diameter of *Perinereis*, exhibiting a positive correlation in the low to moderate salinity range (0.28–3.97 PSU). *Perinereis* growth plateaus when salinity exceeds a threshold of approximately 18 PSU, indicating a physiological tolerance limit. (3) Burrow diameter and sediment bioturbation exhibit no significant correlations with sediment grain size, salinity, turbidity or total organic carbon content. This may be attributed to infaunal interactions (e.g. associations with *Macrophthalmus japonicus*) and the combined influence of multiple environmental factors. This study improves our understanding of the

biology and ichnology of modern *Perinereis* traces. It provides a quantitative basis for interpreting the interactions between infauna and their environment in intertidal flat ecosystems.

**KEYWORDS:** DELTAIC TIDAL FLAT, NEOICHOLOGY, *PERINEREIS*, PHYSICOCHEMICAL FACTORS, PALEOENVIRONMENT

## 1 INTRODUCTION

2 Neoichnology focuses on the interactions between modern organisms and sediments,  
3 integrating research findings from the fields of biology, sedimentology and paleontology  
4 (Dashtgard, 2011a, b; Knaust and Bromley, 2012; Adikaram et al., 2017; Kumar, 2017; Brown et al.,  
5 2024). It provides a theoretical framework for analyzing infauna and their burrowing behaviors.  
6 This facilitates an understanding of the dynamic relationships between infaunal activities and  
7 physicochemical factors. Studies of biogenic structures in modern tidal flats may reveal the  
8 relationship between such structures and the physicochemical factors of coastal zones. They may  
9 also be used to tentatively reconstruct sedimentary and environmental conditions during biological  
10 colonization by analyzing burrow characteristics (Virtasalo et al., 2011; Benkhedda et al., 2021).  
11 Particularly in tidal flat areas near estuaries, bioturbation patterns typically reflect gradient changes  
12 in sediment grain size, salinity, and turbidity associated with freshwater input (Buatois et al., 2012,  
13 2019; Demircan and Uchman, 2016; Sendra et al., 2019; Moyano et al., 2020; Morelle et al., 2024).  
14 Although considerable progress has been made in understanding these relationships over recent  
15 decades (Buatois and Mángano, 2011; Dashtgard, 2011a, b; Ayranci et al., 2014; Wang et al., 2019,  
16 2024, 2025), there remains a need to extend neoichnological research to understudied taxa in  
17 regions worldwide, given the inherent variability of trace makers and the complexity of  
18 environmental conditions.

19 The physicochemical gradients of deltaic tidal flats create a dynamic and highly stressful  
20 environment that exerts a strong selective influence on infaunal communities and their biogenic  
21 sedimentary structures (Passarelli et al., 2012, 2014). Polychaetes are fundamental bioturbators in  
22 such environments. Unlike predators or filter feeders, they can disrupt the chemical balance of  
23 sediments through feeding, digestion, excretion, and transporting sediments. They can also  
24 migrate through deep sediments, excrete nitrogen, and reconstruct microbial communities by  
25 transporting intestinal bacteria. These activities are crucial in driving sediment biogeochemical  
26 processes (Cournane et al., 2010; Koo and Seo, 2017; Fang et al., 2018). Previous studies have  
27 extensively investigated the relationships between the morphological characteristics of benthic  
28 organisms and the distribution of their burrows, as well as the relationships between these  
29 characteristics and physicochemical factors. For instance, Wang et al. (2025) found that in the Pearl  
30 River Delta (PRD), the burrows of *Macrophthalmus japonicus* are more complex and their  
31 bioturbation is more intense in environments with fine-grained substrates, high TOC content,  
32 freshwater to lower mesohaline salinity, and suitable turbidity. Olabarria et al. (1998) observed that  
33 the dominant bivalve organisms in the Rías Bajas in northwestern Spain are more prevalent in  
34 coarse sand and gravel substrates, as well as in the intertidal zone and in fine sand substrates with  
35 an organic matter content of 1–2%. Rowshan et al. (2023) showed that polychaete abundance is  
36 higher and the community structure is more dominant in silty loam substrates, environments with  
37 high total organic matter (TOM) content, and high salinity in the shallow waters of the southern  
38 Caspian Sea, Iran. *Perinereis* are widely distributed across the tidal flat burrow systems of the Pearl  
Ocean and Coastal Research, 2026, v74 (in press)

39 River Delta (PRD) (Wang et al., 2019; Pang et al., 2021). However, research into the burrows of this  
40 species in the PRD is currently limited, particularly with regard to systematic quantitative analysis of  
41 the relationship between burrow characteristics and environmental physicochemical factors. This  
42 makes *Perinereis* an ideal model organism for exploring how deltaic environments regulate biogenic  
43 sedimentary structures.

44 Traditional burrow casting and excavation methods can destroy the original structure of  
45 burrows. However, computed tomography (CT) technology can analyze their complex morphology  
46 efficiently, providing a reliable way to link bioturbation structures to physicochemical factors (Mazik  
47 et al., 2008; Herringshaw et al., 2010; Pennafirme et al., 2019; Howman et al., 2024). This study  
48 employed CT scanning and three-dimensional reconstruction technology to systematically and  
49 quantitatively analyze the surface traces and morphological characteristics of *Perinereis* burrows in  
50 the tidal flats of the Pearl River Delta (PRD). The study will address the following three scientific  
51 questions in depth: (1) explore the morphological and structural characteristics of surface traces  
52 and dwelling burrows of *Perinereis* in the tidal flats of the Pearl River Delta; (2) clarify the regulatory  
53 effects of physicochemical factors such as sediment grain size, salinity, turbidity, and TOC content  
54 on the burrow diameter and bioturbation behavior of *Perinereis*. and (3) reveal the patterns  
55 underlying the community distribution of *Perinereis* under the comprehensive influence of  
56 multi-factor synergy and biological interactions.

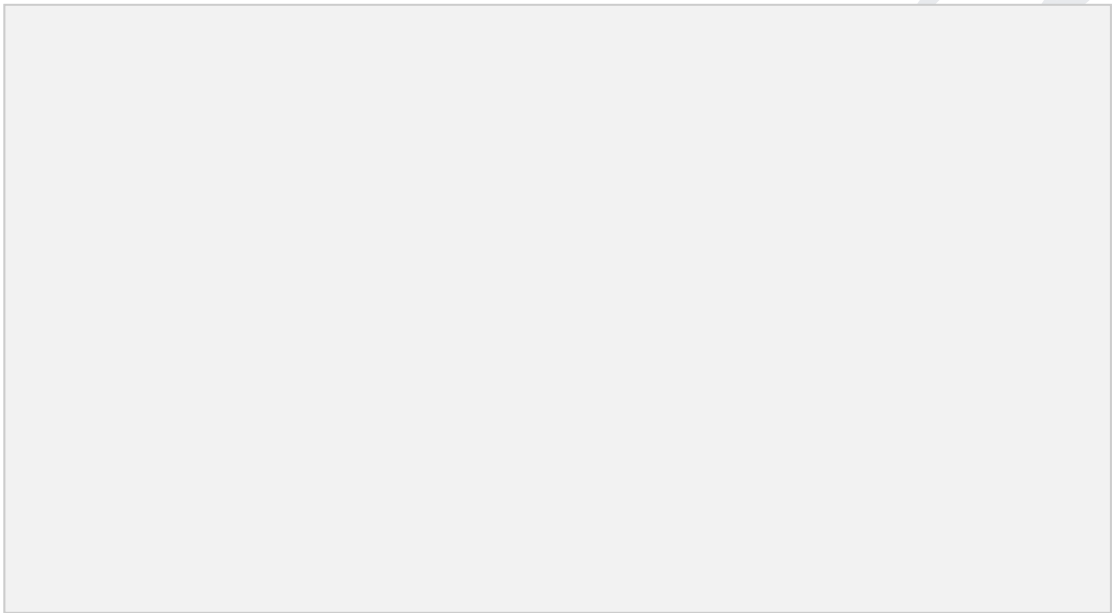
57

## 58 METHODS

### 59 Study Area

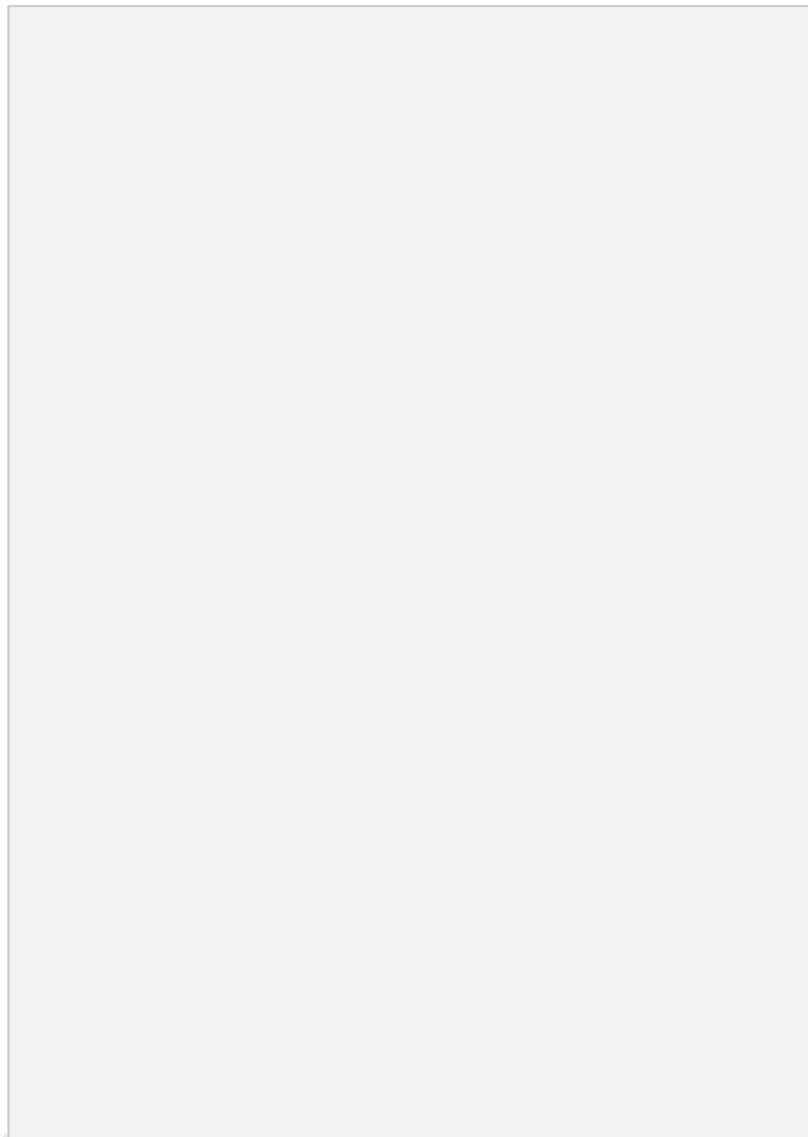
60 Along the northern coast of the South China Sea, the research area covers the delta-plain tidal  
61 flats of the Pearl River Delta (PRD) in southern China, as well as adjacent nearshore islands (Figs.  
62 1A-C). The complex river network of the PRD discharges an average annual water volume of  
63 approximately  $2823 \times 10^8$  m<sup>3</sup> and a sediment load of  $72.4 \times 10^6$  t (Liu et al., 2014), discharging into  
64 the South China Sea through eight estuarine outlets, namely Humen, Jiaomen, Hongqimen,  
65 Hengmen, Modaomen, Jitimen, Hutiaomen, and Yamen. All the estuaries in the study area are tidal.  
66 They are characterized by an irregular semi-diurnal tidal cycle, with two flood and two ebb tides per  
67 day. Each lunar month includes six days of spring tides and six days of neap tides, with the  
68 remainder being intermediate tides. The tidal range is generally between 0.86 m and 1.66 m,  
69 classifying the region as microtidal (Zhang et al., 2010, 2017). The study area is located in a coastal  
70 region south of the Tropic of Cancer with a subtropical monsoon climate. It has a warm and humid  
71 subtropical monsoon climate, with an annual average temperature of 21.5–22.5°C, which meets the  
72 classification standard for a subtropical climate (annual average temperature  $\geq 20^\circ\text{C}$ ). The annual  
73 average precipitation exceeds 1600 mm, resulting in abundant rainfall (Wei et al., 2024). Sampling  
74 took place during the winter, from December 2021 to February 2022. The annual average rainfall in  
75 the study area exceeds 1,600 mm (Wei et al., 2024), and there are pronounced seasonal variations  
76 in hydrological variables. Peaks in summer precipitation ( $900 \pm 120$  mm) and runoff ( $1.35 \pm 0.20 \times$   
77  $10^8$  m<sup>3</sup>) occur first, followed by peaks in spring ( $350 \pm 50$  mm,  $0.45 \pm 0.08 \times 10^8$  m<sup>3</sup>), autumn ( $250 \pm$   
78  $40$  mm,  $0.30 \pm 0.07 \times 10^8$  m<sup>3</sup>) and winter ( $100 \pm 20$  mm,  $0.15 \pm 0.05 \times 10^8$  m<sup>3</sup>), in descending order (Li

79 et al., 2020; Xiao and Cui, 2021). Precipitation is highly concentrated in summer, resulting in  
80 significant variability in river discharge and tidal currents. The wet season is characterized by strong  
81 hydrodynamics, enriched nutrients and frequent scouring of benthic organisms, whereas the dry  
82 season features weaker hydrodynamics, increased salinity and abundant aquatic vegetation (Feng  
83 et al., 2021; Pang et al., 2021; Yang et al., 2022). The bay contains numerous remnant hills and  
84 islands, which form natural barriers at the estuary mouths and effectively attenuate wave energy.  
85 Consequently, wave action is generally weak, with an average wave height of approximately 1 m (Jia  
86 et al., 2016). Intense weathering in the source regions supplies fine-grained sediments to the river  
87 systems. the total annual input of fine-grained sediment transported, deposited, and dispersed  
88 within the estuaries and adjacent coastal and shelf areas of the South China Sea exceeds  $8400 \times 10^4$   
89 t (Chen et al., 2023).



90  
91 **Figure 1** - Study area. (A) Map of China, red star marks the study area; (B) map of the Pearl River Delta; (C)  
92 satellite image showing the tidal flat that forms the study area (image source: <http://glovis.usgs.gov/>).

### 93 **Sampling**



94

95 **Figure 2** - Position of stations and surface-sediment distribution on the studied tidal flat of the Pearl River

96 Delta; red stars mark stations where *Perinereis* burrows were present.

97 Sampling was conducted with Qiao Island as the central point: Underwater sampling was

98 conducted along radial transects, each measuring 12–20 km in length. A total of 63 sampling stations

99 were established across the study area for sedimentological and ichnological analysis (Fig. 2).

100 Sediment samples were collected using vertical coring with PVC tubes that are 15 cm in length and 7.5

101 cm in diameter. Bioturbation areas were avoided during sampling, and the pipe mouths were sealed

102 after collection to preserve the morphology of burrows. Surface sediments were collected at a depth

103 of 0-5 cm below the sediment surface, and two parallel samples were prepared. These samples were

104 sealed and stored in sterile polyethylene bags for analysis of indicators such as particle size and total

105 organic carbon (TOC). Two parallel surface water samples were also collected and sealed in 100 ml

106 plastic bottles for later use to determine parameters such as salinity and turbidity. All samples were

107 stored at ambient temperature in light-proof conditions to preserve their original composition before

analysis. To collect well-preserved, representative biogenic sedimentary structures, 15 cm-long PVC core tubes with an inner diameter of 7.5 cm were pressed into the sediment during low tide to collect samples in situ. The cores were then sealed within the tubes to create an anoxic environment that would effectively inhibit bioturbation. According to the density of *Perinereis* burrows in the substrate, 35 sediment cores were collected in varying quantities from 18 sampling stations. Six stations with typical sedimentary environments where *Perinereis* were found were selected for sampling according to the distribution characteristics of tidal flat microenvironments in the Pearl River Delta (PRD). The exact locations of these stations were determined using a handheld GPS device and marked on Google Earth Pro. Columnar samples were collected in accordance with the principles of covering the tidal flat microenvironments and ensuring the representativeness of the samples. Meanwhile, points with well-preserved, morphologically typical *Perinereis* burrows were selected to meet the requirements of subsequent experiments such as CT scanning and three-dimensional reconstruction. The number of columnar samples collected and the specific coring points were mainly determined by the integrity of the preservation and representativeness of the *Perinereis* burrows, as well as the characteristics of microenvironmental disruption at each station. Only points with complete burrow morphology that were easy to collect and difficult to damage were sampled using PVC pipes.

124

### 125 Grain Size Analysis

126 A total of 58 surface sediment samples for grain size analysis were collected from the 63  
127 sampling stations (Table 1). The depth of the core samples is 0–15 cm, with one or two cores collected  
128 at each sampling point. For well-preserved, representative *Perinereis* burrows, additional directional  
129 core sampling was conducted using PVC pipes with a diameter of 5 or 7.5 cm and a height of 15 cm.  
130 The sediment at station 63 consisted of gravel, while stations 17, 53, and 55 were characterized by  
131 coarse sand sediments, both of which render them unsuitable for our grain size analytical  
132 instrumentation. Furthermore, sampling at station 43 was hindered by excessive current velocities,  
133 which prevented successful underwater sampling operations. All sediment samples were oven-dried  
134 at 105°C for 24 hours, and approximately 0.2 g of each sample was transferred to pre-cleaned glass  
135 beakers. To remove organic matter, 10% hydrogen peroxide (H<sub>2</sub>O<sub>2</sub>) was added, followed by 10%  
136 hydrochloric acid (HCl) to eliminate carbonates. Following chemical pretreatment, samples were left to  
137 settle. Before analysis, a 0.5% calgon solution was added to disperse the clay and silt-sized particles,  
138 and the suspensions were ultrasonicated for 10 minutes (40 kHz) to ensure complete disaggregation.  
139 The grain size test was performed using a Mastersizer 2000 (Malvern Instruments Ltd.,  
140 Worcestershire, UK), with triplicate measurements performed for each sample to ensure  
141 reproducibility (Bertrand et al., 2014; Li et al., 2021; Song and Li, 2023).

142 **Table 1** - Grain size parameters (mean grain size, standard deviation (SD), and skewness), turbidity (in  
143 nephelometric turbidity units (NTU), salinity (in parts per thousand) and total organic carbon content  
144 (TOC) samples taken from the Pearl River Delta.

Station	Mean Grain Size(mm)	SD (mm)	Skewness	Turbidity (NTU)	Salinity (PSU)	TOC (%)
1	0.37	0.64	0.12	8.36	30.10	
2	0.35	0.68	0.02	8.15	31.80	

3	0.39	0.61	0.10	7.45	31.80	
4	0.01	0.32	0.12	12.02	12.90	
5	0.02	0.16	-0.06	6.24	11.80	0.40
6	0.01	0.28	0.06	15.53	20.90	1.01
7	0.01	0.28	0.10	5.79	21.60	0.94
8	0.01	0.26	0.03	2.68	23.50	1.03
9	0.01	0.17	-0.23	10.65	26.90	0.85
10	0.26	0.52	0.26	40.32	28.11	
11	0.01	0.24	0.05	45.88	11.80	1.03
12	0.01	0.29	0.13	6.40	18.30	1.16
13	0.01	0.22	-0.04	5.85	20.40	0.92
14	0.01	0.27	0.04	2.44	21.30	0.77
15	0.01	0.28	0.08	3.74	21.00	0.78
16	0.01	0.34	0.17	10.20	17.40	1.18
17				15.63	18.10	1.41
18	0.01	0.35	0.12	12.02	18.80	1.00
19	0.01	0.36	0.16	5.11	18.20	1.03
20	0.01	0.35	0.16	3.90	19.20	1.56
21	0.01	0.25	-0.01	6.94	18.60	1.04
22	0.01	0.20	-0.03	7.00	18.90	0.82
23	0.01	0.18	-0.08	2.69	20.70	0.25
24	0.05	0.18	0.59	3.33	22.00	0.20
25	0.01	0.22	0.07	1.67	22.30	0.57
26	0.01	0.25	-0.02	31.52	20.20	0.83
27	0.01	0.29	0.09	13.94	22.10	0.94
28	0.01	0.28	0.07	6.37	25.00	1.57
29	0.03	0.13	0.04	8.49	26.40	0.99
30	0.01	0.29	0.12	6.07	26.50	1.19
31	0.01	0.33	0.11	34.44	16.20	1.63
32	0.01	0.32	0.09	33.60	15.90	1.24
33	0.01	0.32	0.15	36.76	10.30	1.54
34	0.01	0.32	0.16	48.96	3.44	1.57
35	0.01	0.29	0.13	16.06	8.13	1.59
36	0.18	0.24	0.66	192.23	15.50	
37	0.01	0.30	0.15	19.63	15.80	1.63
38	0.01	0.27	0.01	6.87	12.60	1.35
39	0.02	0.17	-0.02	5.01	9.31	0.55
40	0.02	0.19	0.06	58.74	14.30	2.18
41	0.02	0.17	-0.00	16.39	0.55	0.74
42	0.02	0.21	0.31	7.54	2.74	1.01
43					6.23	
44	0.46	0.71	0.03	75.98	16.80	

45	0.31	0.64	0.00	142.07	18.00	0.53
46	0.10	0.20	0.52	215.27	12.40	0.90
47	0.46	0.71	0.02	11.41	11.30	
48	0.01	0.32	0.08	163.00	5.48	1.91
49	0.02	0.10	-0.31			1.50
50	0.36	0.68	0.02	148.03	13.90	
51	0.31	0.62	0.02	11.38	10.60	
52	0.25	0.61	0.02	113.90	14.10	
53				192.57	13.60	
54	0.25	0.58	-0.04	129.90	14.20	
55				158.73	11.60	
56	0.02	0.21	0.10	240.27	2.17	0.67
57	0.02	0.25	0.24	44.47	0.28	1.42
58	0.04	0.13	0.06	42.88	0.47	1.38
59	0.01	0.36	0.22	347.17	2.19	2.40
60	0.01	0.35	0.21	117.63	3.97	0.60
61	0.01	0.36	0.16	118.07	9.27	1.58
62	0.01	0.28	0.09	68.42	2.20	2.72
63				116.67	12.10	3.70

## 145 Determination of Turbidity, Salinity, and Organic Matter Content

146 Water samples were collected at 62 sampling stations during low tide for salinity and turbidity  
147 measurements. Stations 49 and 50 have hydrological connectivity within the same water body;  
148 therefore, only Station 50 was sampled. Salinity was measured using an SX813 conductivity meter and  
149 recorded in Practical Salinity Units (PSU). Each point was measured at least three times, and the  
150 average value was taken to reduce the impact of instantaneous fluctuations and operational errors.  
151 The difference between the three readings had to be less than 0.002 PSU. Turbidity was measured  
152 using an NS-type turbidity meter and expressed in nephelometric turbidity units (NTU). Each sample  
153 was measured repeatedly at least three times, and the average value was taken as the final result.

154 Total organic carbon (TOC) content was analyzed from sediment samples taken at 48 stations  
155 (Table 1). According to Shetty and Goyal (2022), the loss-on-ignition (LOI) method was used to  
156 determine the total organic carbon (TOC) content. The dried samples were ground using a mortar and  
157 pestle, further dried for 30 hours at 60 °C, and then heated to 550 °C for 4 hours. The loss in weight  
158 from organic matter combustion during LOI was measured using an electronic balance with a  
159 precision of  $\pm 0.001$  g (Wang et al., 2025). Triplicate measurements were performed for each sample,  
160 with a relative standard deviation (RSD) < 5% ensuring analytical reproducibility.

161

## 162 Computed tomography (CT) scanning

163 All 35 collected cores were temporarily stored for one month under ambient temperature, dry,  
164 and light-protected conditions. After the completion of all field sampling, they were taken to Nanjing  
165 Institute of Soil Research, Chinese Academy of Sciences, for computed tomography (CT) scanning.  
166 During transport to the laboratory for scanning, all core tubes were maintained in a strictly upright  
167 position to prevent disruption and resuspension of sediments. The Nanotom S CT scanner was

168 employed with the following parameters: voltage 180 kV, power of 15 W, resolution of 200 nm (0.2  
 169  $\mu\text{m}$ ), and 3D magnification ranging from 1.5-100 $\times$ . During scanning, the X-ray source emitted a  
 170 collimated beam while the core was rotated 360 $^\circ$  to acquire multi-angular projections of the target  
 171 specimen. A total of 4575 projection images were collected per sample, with each 250 ms projection  
 172 averaged over 8 frames (2 seconds per projection), totaling approximately 153 minutes per scan. Ring  
 173 artifact correction was enabled to improve image quality.

174 All three-dimensional reconstructions were completed at the Nanjing Institute of Geology and  
 175 Paleontology, Chinese Academy of Sciences. To minimize file sizes and reduce computational burdens,  
 176 the reconstructed 3D volumes were converted to an 8-bit image format using Fiji-ImageJ software.  
 177 Subsequently, these processed images were imported as a 3D project into VG Studio MAX (Version  
 178 2.1, Volume Graphics GmbH, Germany), where a 3D non-linear digital median filter with  
 179 edge-preserving properties was applied. This filter adopted a 5-voxel window size to mitigate image  
 180 noise. The final scanned volume exhibited a 3D voxel size of 30  $\mu\text{m}$ . For the sediment core samples,  
 181 regions of interest (ROIs) that contained burrow structures were segmented via a threshold-based  
 182 seed point growing algorithm, which enabled the generation of a 3D visualization of the burrow  
 183 network (Nel et al., 2001; Petrash et al., 2011; Hale et al., 2015; Mimier & Żbikowski, 2017).

184

## 185 **Neoichnological assessment**

186 According to field observations and CT image analysis, traces of biological disruption by  
 187 *Perinereis* was found at only six out of 63 sampling stations *Perinereis* (Table 2). At each station, five 1  
 188 m  $\times$  1 m quadrats, each with a depth of 20 cm, were randomly excavated. To provide a physical  
 189 reference scale, a ruler was placed on the surface of the sediment, after which photos of the sediment  
 190 surface were taken to record the burrow morphology. The average burrow density was determined by  
 191 counting the number of trace producers and calculating the average. ImageJ software was then used  
 192 to measure the diameter and cross-sectional area of individual burrows. The occupied surface area  
 193 ( $\text{cm}^2/\text{m}^2$ ) at each station was obtained by multiplying the average burrow density by the total average  
 194 cross-sectional area. This value was then used to quantify the sediment bioturbation intensity caused  
 195 by the *Perinereis*. The sediment bioturbation rate (%), according to Dashtgard (2011a), is calculated as  
 196 (average burrow cross-sectional area  $\times$  average burrow density)  $\times$  0.01. Additionally, the influence of  
 197 physicochemical factors on average burrow diameter was investigated, as were their correlations.  
 198 Logistic nonlinear least-squares regression was performed in Origin software to model the  
 199 relationship between average burrow diameter and salinity. The significance of the model and its  
 200 parameters was evaluated using ANOVA and t-tests, respectively. The goodness of fit was represented  
 201 by  $R^2$  and adjusted  $R^2$  ( $P < 0.05$ ).

202 **Table 2** - Quantification of *Perinereis* bioturbation: burrow morphometrics (diameter, cross-sectional  
 203 area, density) and calculated sediment disruption (%) across sampling stations on the Pearl River Delta

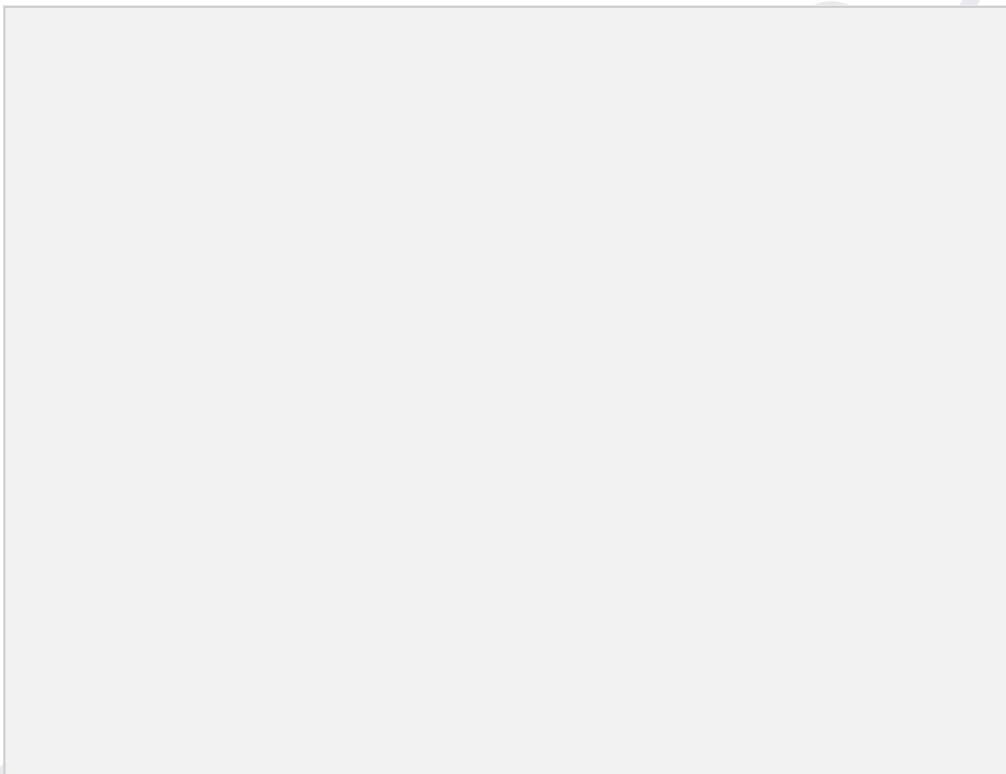
Station	Average burrow diameter (cm)	Average burrow cross-sectional area ( $\text{cm}^2$ )	Average burrow density (number of burrows/ $\text{m}^2$ )	Cross-sectional area* burrow density ( $\text{cm}^2/\text{m}^2$ )	Sediment disruption (area)%
---------	------------------------------	-------------------------------------------------------	-----------------------------------------------------------	-------------------------------------------------------------------	-----------------------------

45	0.336	0.089	208	18.5	0.19
56	0.256	0.051	4900	250	2.50
57	0.102	0.008	300	2.4	0.02
58	0.157	0.019	7900	150	1.50
60	0.257	0.052	5100	265.2	2.65
62	0.353	0.098	2800	274.4	2.74

204

## 205 RESULTS

### 206 Sedimentology



207

208 **Figure 3** - Mean grain size and sorting values for all samples collected at the tidal flat; red stars denote  
209 samples from stations where *Perinereis* was present.

210 Overall, *Perinereis* was predominantly found in fine-grained substrates, such as silt, clay, and silty  
211 sand (Fig. 2), all of which exhibit poor sorting (sorting index > 1; Fig. 3).

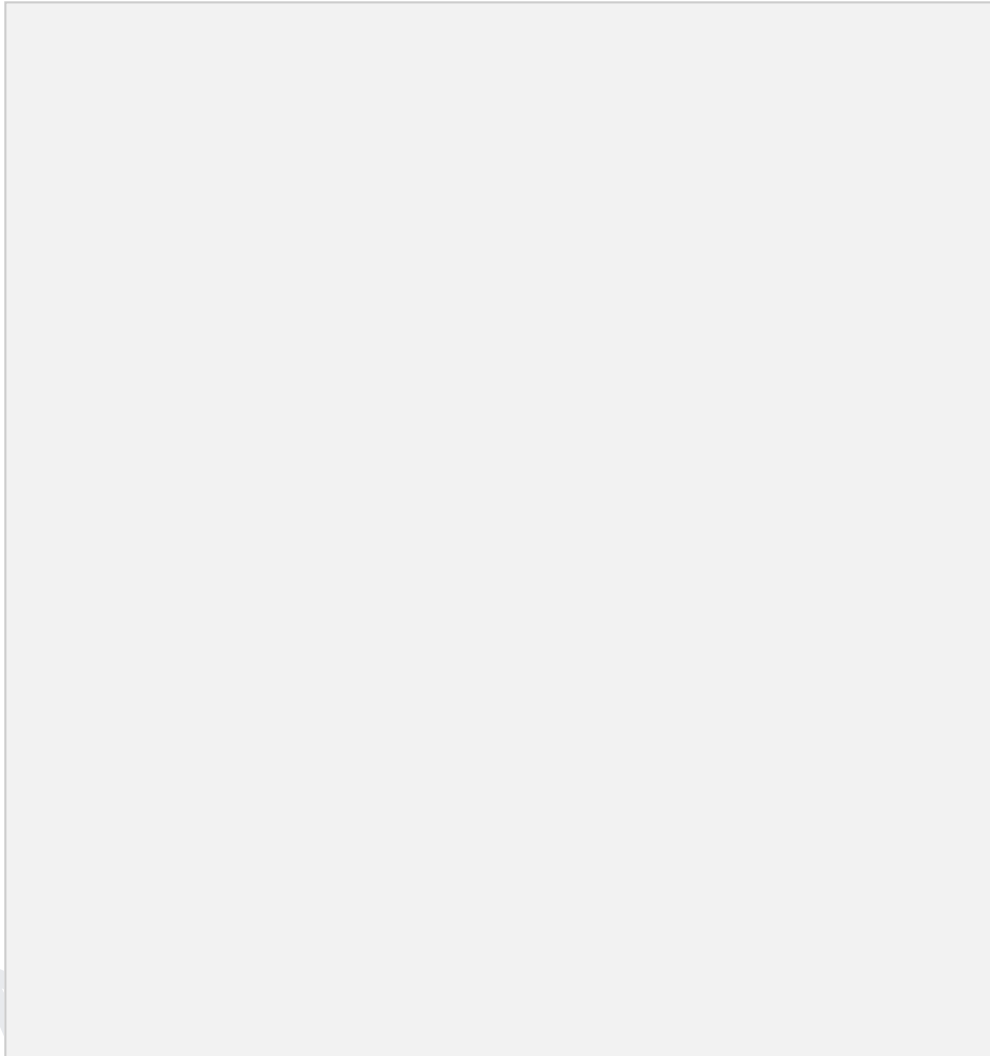
212 The upper intertidal zone of the study area is characterized by poorly sorted muddy sediments,  
213 with arcuate ridge ripples (Fig. 4A) and soft-sediment deformation structures present. The dense  
214 reeds and shrubs surrounding the muddy tidal flat (Fig. 4B) provide abundant organic matter for  
215 benthic organisms, leading to the formation of numerous burrow openings on the sediment surface.

216 The middle intertidal zone mainly consists of poorly sorted silty sediments and features typical  
217 tidal bedding, including lenticular bedding, flaser bedding and ripple cross-bedding. Meandering tidal

218 creeks traverse the intertidal zone (Fig. 4C) and transport fine-grained suspended sediments during  
219 flood tides. These sediments are subsequently deposited during ebb tides, forming extensive muddy  
220 deposits. Scattered shallow pools filled with water are also common in this zone.

221 The lower intertidal zone is characterized by well-sorted sandy sediments ranging from medium to  
222 fine sand (mean grain size: 0.1–0.5 mm). Various sedimentary structures have formed in these sandy  
223 deposits, including parallel bedding (Fig. 4D), trough cross-bedding and current ripples (Fig. 4E).

224 Oscillation ripples were also clearly visible at the Dong'ao Island site (Fig. 4F).



225  
226 **Figure 4** - Sedimentological features on the studied intertidal flat. (A) Curved ridge ripple in silty mud  
227 (station 53). (B) the mudflat with dense shrubs and reeds, featuring a high density of burrow openings  
228 (white arrows with black outline) (station 59). (C) The meandering tidal creeks (indicated by the yellow  
229 arrows) traverse the intertidal flat, and there are many small water-filled pools (indicated by the white  
230 arrows) on the surface of the middle intertidal flat (station 49). (D) sandy parallel bedding (station 10).  
231 (E) current ripples (station 45). (F) oscillation ripples (outlined by white dashed line) (station 2).

232

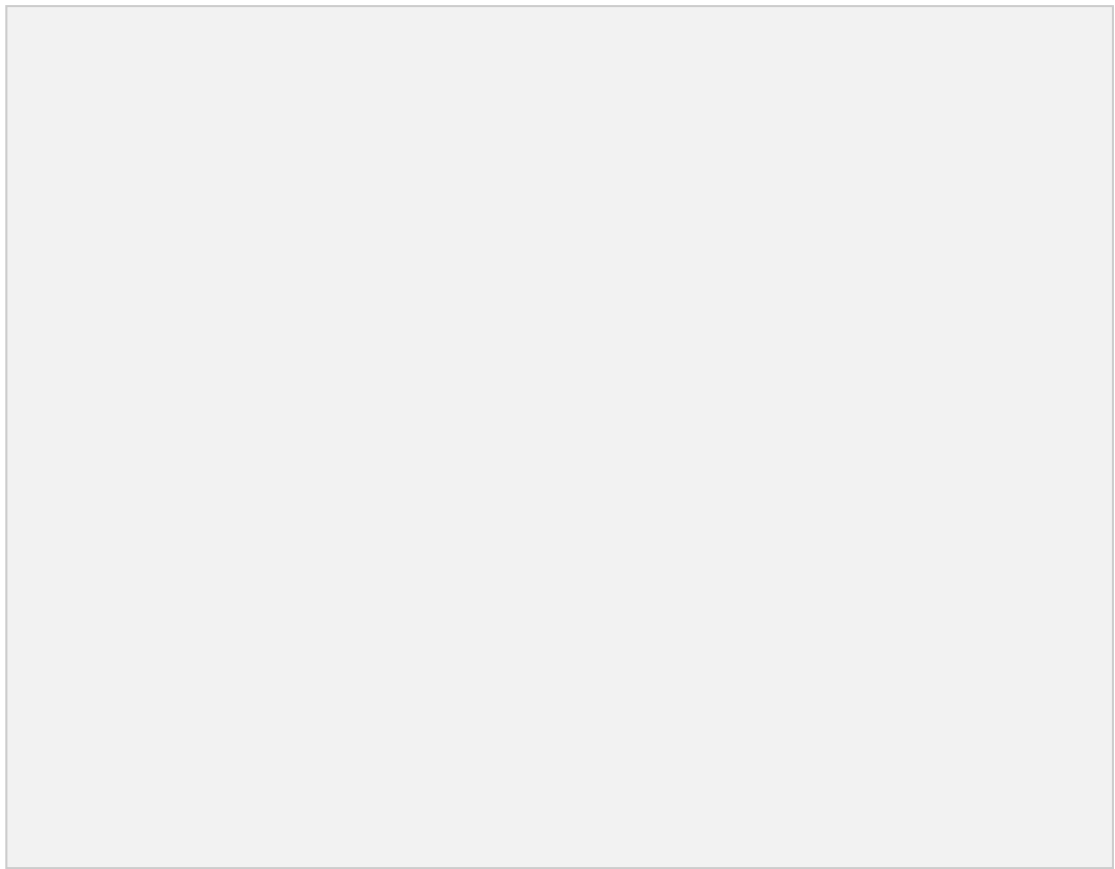
### 233 **Physicochemical factors**

234 The physicochemical factors measured include salinity, turbidity, and total organic carbon (TOC)  
235 content. Salinity increases gradually from the west to the east and decreases from the south to the  
236 north. Overall, the study area is dominated by saltwater and brackish environments, with only a few  
237 stations (Stations 41, 57 and 58) showing significantly lower salinity due to the input of freshwater  
238 from the land. According to salinity, the area can be divided into three categories: oligohaline (< 0.05  
239 Practical Salinity Units (PSU)), mesohaline (0.05–16 PSU), and polyhaline (> 16 PSU), with respective  
240 means and standard deviations of  $0.38 \pm 0.13$ ,  $9.68 \pm 4.76$ , and  $22.04 \pm 4.40$ .

241 Turbidity can serve as an indicator of terrestrial inputs (e.g., riverine sediment transport) and  
242 hydrodynamic sorting processes. The water in the tidal flats of the study area is generally turbid, with  
243 turbidity gradually increasing from the sea to the land (from east to west). There is, however, no  
244 obvious systematic change along the north-south transect (Fig.5B). According to turbidity, the water  
245 can be divided into four categories: <20 NTU, 20–80 NTU, 80–170 NTU and >170 NTU. Their respective  
246 means and standard deviations are  $8.37 \pm 4.57$ ,  $46.83 \pm 14.11$ ,  $134.22 \pm 19.23$  and  $237.50 \pm 64.42$ .

247 Total organic carbon (TOC) content ranges from 0.20% to 3.70%, with most stations falling within  
248 the 0.40% to 2.00% range, indicating an overall low to moderate level of organic matter. The highest  
249 TOC content (3.70%) occurs at station 63, and the lowest (0.20%) at station 24 (Table 1), reflecting  
250 significant spatial variability in organic matter enrichment. High TOC values are mostly found in areas  
251 strongly influenced by terrestrial inputs and relatively low salinities (2.17–14.30 PSU). In contrast, low  
252 TOC values are concentrated at station 23 (0.25%) and station 24 (0.20%), as well as some high-salinity  
253 stations.

254 Analysis of the relationship between the burrow characteristics of *Perinereis* and environmental  
255 factors reveals a significant correlation between burrow diameter and salinity. Burrow diameter  
256 increases with rising salinity between 0.28 and 3.97 Practical Salinity Units (PSU), stabilizing above  
257 approximately 18 PSU (Fig. 9). At salinities of 0.5–16 PSU, the degree of sediment bioturbation  
258 decreases as salinity increases (Fig. 10D). However, burrow diameter and sediment bioturbation show  
259 no significant correlations with TOC content, mean grain size or turbidity (Figs. 10A–C).



260

261 **Figure 5** - Salinity (A) and turbidity (B) values measured at all stations on the Pearl River Delta tidal flat;  
262 red stars denote stations where *Perinereis* was present.

263

### 264 **Neoichnology of *Perinereis***

265 Surface traces and dwelling burrows constructed by *Perinereis* mainly occur in the modern  
266 intertidal zones of the Pearl River Delta (PRD). Their detailed characteristics are described below.

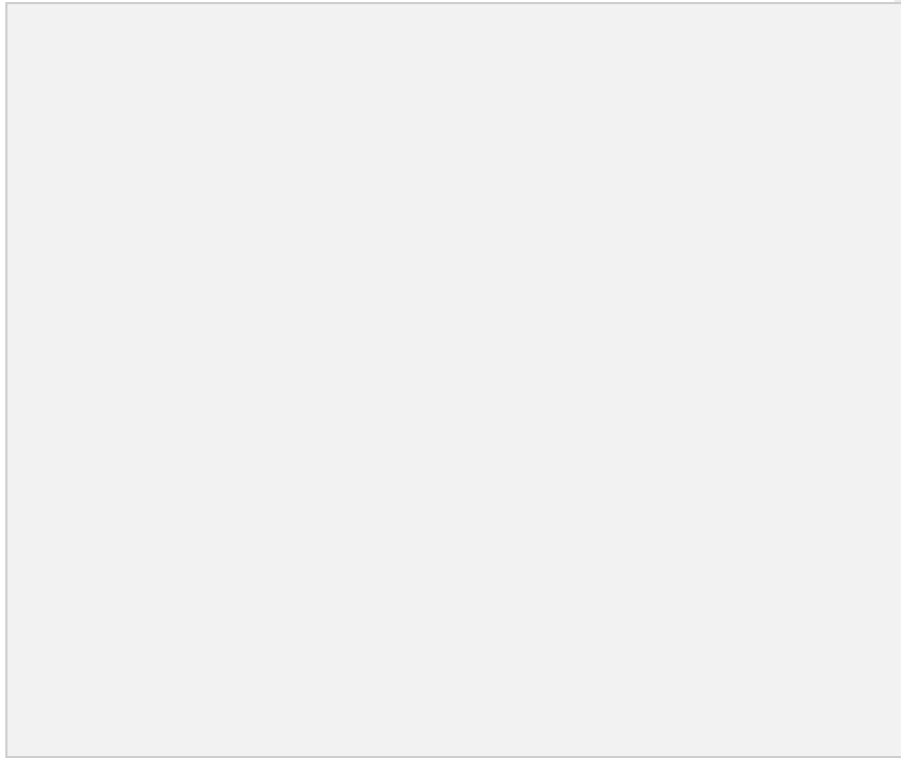
267 Upper intertidal zone: On the sediment surface, the fecal pellets of *Perinereis* appear as slender,  
268 cylindrical, curved accumulations, measuring around 1 mm in width (Fig. 6D). Their burrow openings  
269 are mostly circular (Fig. 6C), measuring 0.5–2 mm in diameter, and the burrows can extend to a depth  
270 of 11 cm below the surface (Figs. 7A and 7B). The red and white arrows in Fig. 7C indicate suspected  
271 dwelling/activity chambers. These burrows are relatively shallow, generally reaching only about 5 cm  
272 below the surface. Three-dimensional images show that the burrows of *Perinereis* consist mainly of  
273 fine, densely packed tunnels forming a highly interconnected network with extensive branching,  
274 bending, and bifurcation (typically at angles of 45–90°). The green arrows in Figs 7G and 7H show  
275 where the tunnels intersect and intertwine. In contrast, the burrows of *Macrophthalmus japonicus* are  
276 mostly Y- or J-shaped, featuring thick main tunnels (5–10 mm in diameter) and multi-directional  
277 branches that form complex connected spaces (Fig. 7C).

278 Middle intertidal zone: A live red *Perinereis*, measuring approximately 10–12 cm in length, was  
279 observed on the sediment surface (Fig. 6A), alongside the circular, 7–10 mm openings of adjacent  
280 *Macrophthalmus japonicus* burrows (Fig. 6B). The two species often coexist at stations where *Perinereis*

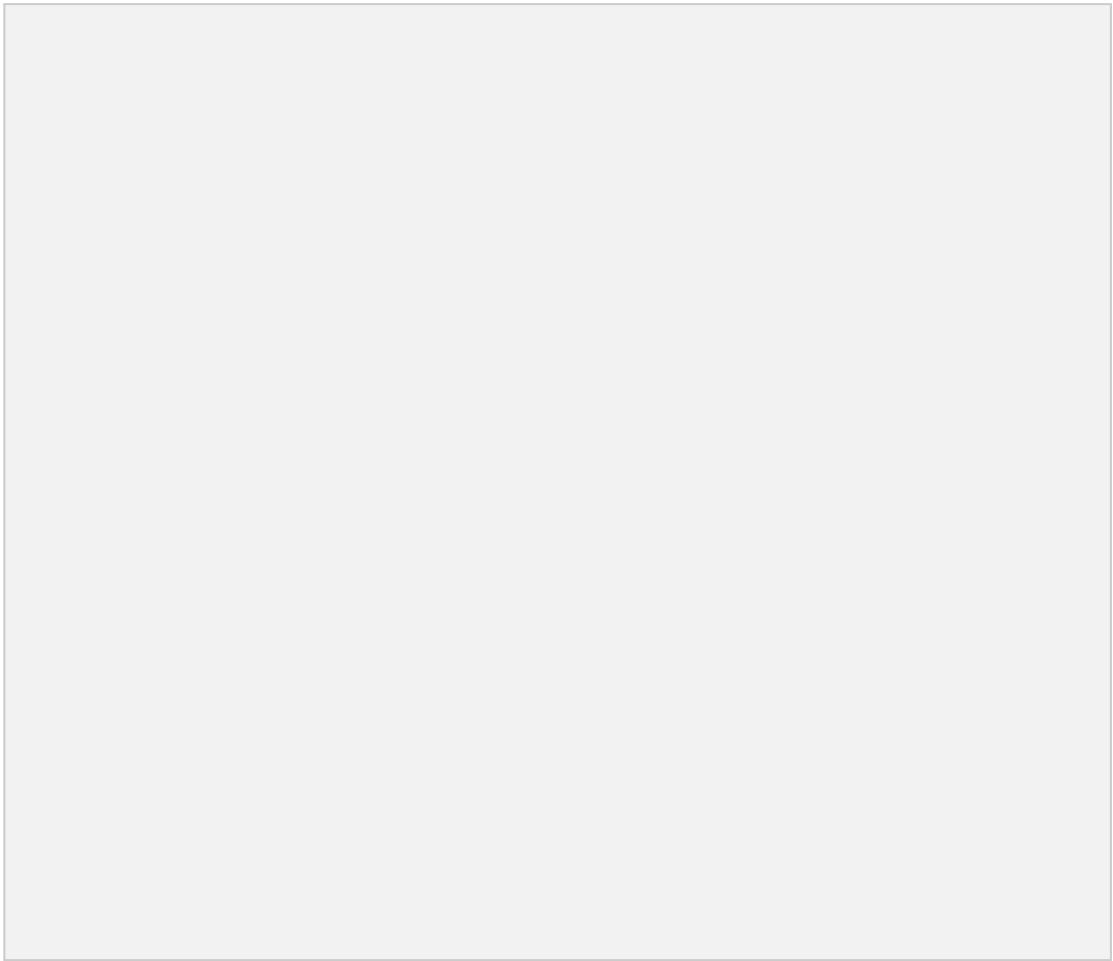
281 occur, with the burrows of *Perinereis* frequently distributed around the Y-shaped burrows of  
282 *Macrophthalmus japonicus* (Figs. 7D and 7E). Some *Perinereis* burrows are also Y-shaped with upward  
283 openings, but they are smaller than the crab burrows. Three-dimensional images show that *Perinereis*  
284 burrows within the sediment are extremely dense (0.5–1 mm in diameter) with occasional swellings at  
285 branch points (Fig. 7F, green arrow).

286 Lower intertidal zone: The substrate consists of sandy sediment mixed with fine gravel. Linear traces  
287 of *Perinereis* can be seen on the surface as slender features measuring around 2 mm in width (Fig. 6E).

288 Due to the strong tidal and wave dynamics, bioturbation structures are poorly preserved and  
289 *Perinereis* burrows and traces are relatively scarce.

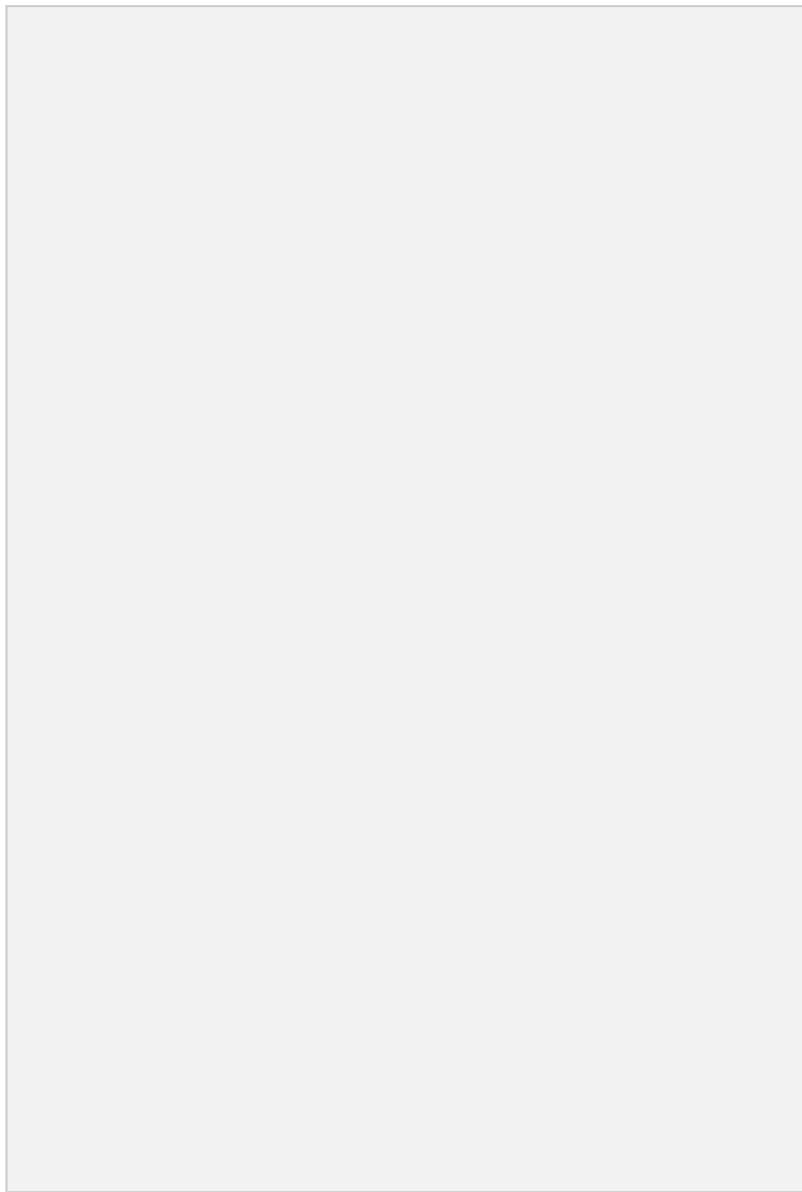


290  
291 **Figure 6** - Traces of *Perinereis* on the sediment surface: surface crawling traces (marked with red  
292 arrows) and openings of subsurface burrows (marked with black arrows). (A) red-colored trace-maker  
293 *Perinereis*. (B) burrow entrance of *M. japonicus*. (C) burrow entrance of *Perinereis*. (D) *Perinereis* faeces.  
294 (E) crawling traces.



295

296 **Figure 7** - CT images of *Perinereis* from the Pearl River Delta intertidal flat. (A), (B) simple *Perinereis*  
297 burrows. (C) simple, rarely branched, nearly vertical burrows of *Perinereis* (marked with red arrow) and  
298 simple J-shaped *M. japonicus* burrow (marked by white arrow). (D) simple *Perinereis* burrows (marked  
299 with red arrow) and simple J-shaped *M. japonicus* burrows (marked by white arrow). (E) complex  
300 *Perinereis* burrows (marked with red arrow) and simple Y-shaped *M. japonicus* burrows (marked by  
301 white arrow). (F) (G) and (H) complex burrows of *Perinereis* with swelling part (marked by green arrow).  
302 Figs. 8A and 8B show field observations of *Perinereis* burrows in sediments. Figs. 8C and 8D are  
303 schematic diagrams of the corresponding morphologies. Simple-type burrows have few scattered  
304 branches and a relatively uniform burrow diameter (Fig. 8D). Their morphologies include U-shaped  
305 and Y-shaped structures. Complex-type burrows (Fig. 8C) have numerous dense branches with  
306 expanded regions at the bifurcations and significant variations in burrow diameter. The combination  
307 of multiple U-shaped and Y-shaped branches, together with dense swollen areas, forms a complex  
308 three-dimensional network that supports the rapid movement and expanded foraging range of  
309 *Perinereis* within the sediment.



310  
 311 **Figure 8** - Comparison of dense burrow openings (A) and sparse burrow openings (B) of *Perinereis* on  
 312 the Pearl River Delta tidal flat; comparison of complex burrows (C) and simple burrows (D).  
 313 **Table 3** - Characteristics of simple and complex burrows across all *Perinereis* stations based on CT  
 314 images.

Station	Morphological structure	swelling phenomenon	symbiotic relationship	Burrow type
45	vertical tubular	no swelling	None	simple
56	vertical tubular and Y-shaped	no swelling	None	simple

57	vertical tubular and Y-shaped	no swelling	None	simple
58	vertical tubular, U-shaped and Y-shaped, multiple branches	with swelling	associated with <i>M. japonicus</i>	complex
60	vertical tubular, U-shaped and Y-shaped	no swelling	associated with <i>M. japonicus</i>	simple
62	vertical tubular, U-shaped and Y-shaped, multiple branches	with swelling	associated with <i>M. japonicus</i>	complex

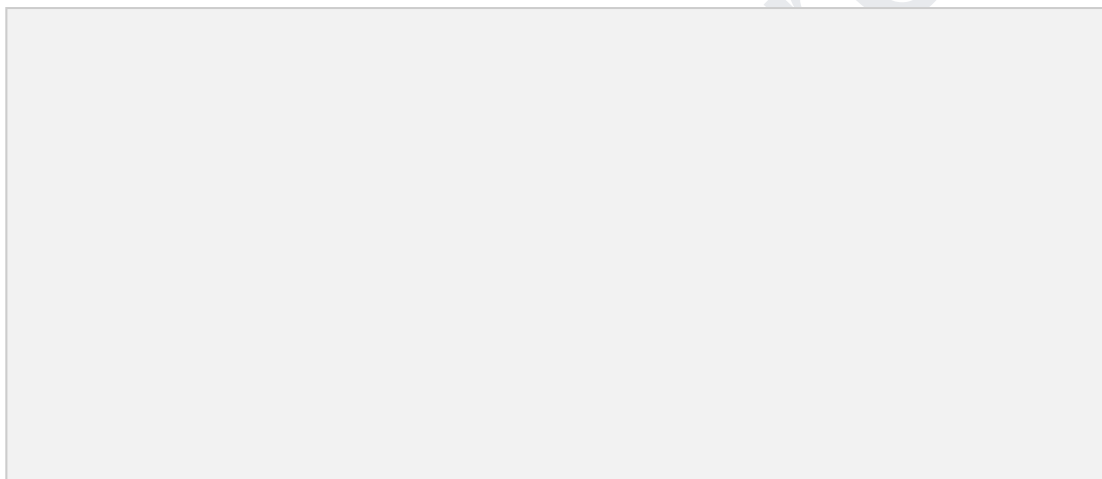
315

## 316 DISCUSSION

317 Analysis of the sediment bioturbation caused by *Perinereis* (Table 2 and Fig. 3) shows that this  
 318 species inhabits fine-grained substrates and exhibits lower burrow density and weaker sediment  
 319 bioturbation in coarser-grained sediments, such as those at Station 45. *Perinereis* can reduce the  
 320 shear resistance of fine-grained sediments through setae movement and mucus lubrication, enabling  
 321 them to burrow efficiently (Nel et al., 2001; Petrash et al., 2011; Mimier and Żbikowski, 2017).  
 322 However, their limited muscle strength and mucus secretion make it difficult for them to penetrate  
 323 medium and coarse sands (Francoeur and Dorgan, 2014; Sun et al., 2019), resulting in a significant  
 324 reduction in burrowing ability. The surface tension of fine-grained substrates is low and burrow  
 325 stability is poor, meaning that *Perinereis* may rely on the stable burrow structures of *Macrophthalmus*  
 326 *japonicus* for survival (Ho et al., 1997; Palomo et al., 2004). However, the bioturbation of *Perinereis* can  
 327 increase sediment porosity, improve the distribution of organic matter, promote microbial activity and  
 328 indirectly provide *Macrophthalmus japonicus* with more benthic microalgae or organic detritus (Palomo  
 329 et al., 2004; Patel and Desai, 2009; Alvarez et al., 2018). This is consistent with the phenomenon  
 330 observed at Stations 58, 60 and 62, where the two species often occur alongside each other. Together  
 331 with the statistics on burrow characteristics in Table 3, it can be inferred that suitable environmental  
 332 conditions and infaunal interactions can improve the settlement success rate of *Perinereis* and  
 333 promote the formation of complex burrows. To a certain extent, this can also weaken the direct  
 334 control of sediment grain size on burrow density (Kruger and Woodin, 1993; Palomo and Iribarne,  
 335 2000)

336 Salinity is an important factor affecting the growth and development of infauna. It can also  
 337 induce spatial heterogeneity by influencing infaunal behavior and distribution (Gingras et al., 2011;  
 338 Ayranci et al., 2013; Freitas et al., 2015; La Croix et al., 2015; Ayranci et al., 2016). In environments with  
 339 fluctuating salinity, *Perinereis* must maintain homeostasis through ion and osmotic regulation. Fig. 9A  
 340 shows a positive overall correlation between salinity and the diameter of individual burrows, with  
 341 each burrow acting as a statistical unit. Data dispersion at the same salinity reflects individual  
 342 differences: each salinity value in the figure corresponds to a single sampling station and the shape  
 343 and color of the data points distinguish the statistical results for burrow diameters from different  
 344 stations. The distribution of burrow diameters at a salinity of 2.20 PSU is the widest, with the largest  
 345 number of data points. This is because low-salinity tidal flat areas are characterized by high levels of

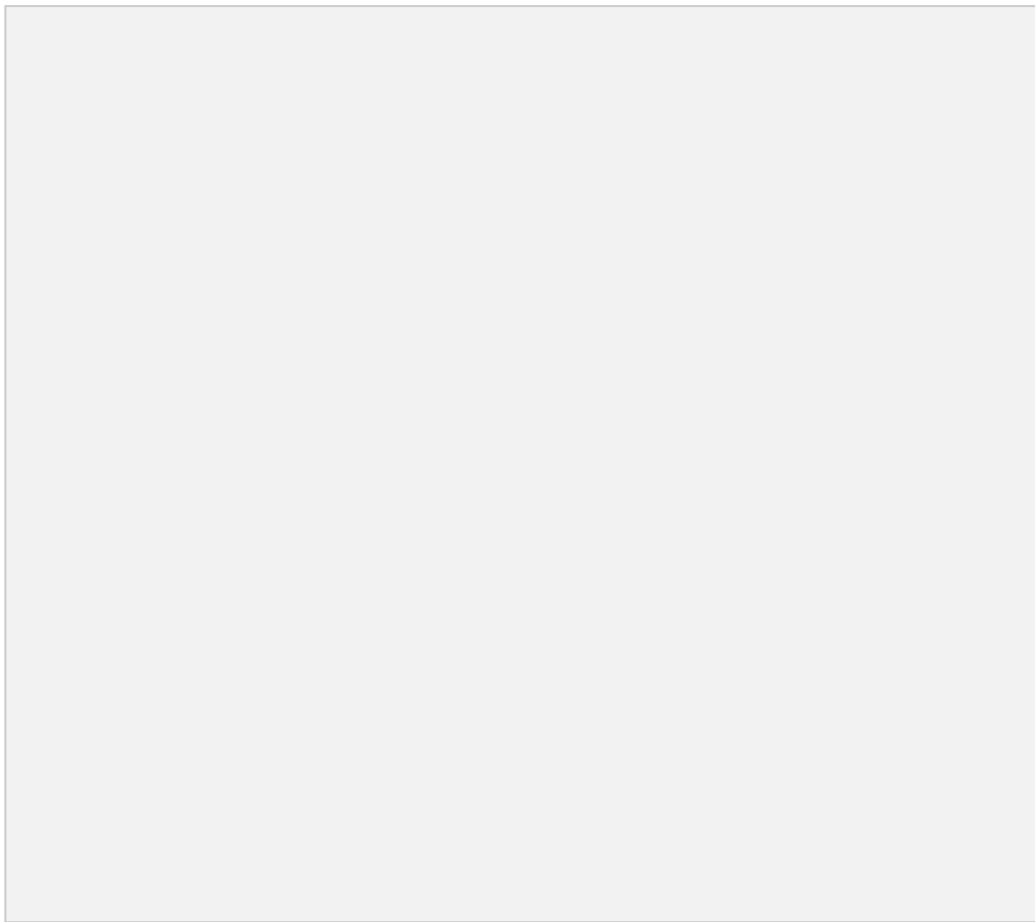
346 organic matter, abundant food resources and relatively low levels of predation. Together, these  
347 factors promote faster growth and larger body size in *Perinereis* individuals, as well as increased  
348 variability in burrow diameter. When salinity increases, the increased osmotic stress may inhibit  
349 growth. However, *Perinereis* tends to develop more advanced tissue structures to meet its  
350 physiological needs. This results in an increase in individual diameter, showing characteristics of  
351 compensatory growth (Pechenik et al. 2016; Villena-Rodríguez et al. 2024). Fig. 9B uses the average  
352 diameter of the burrows at each station as the statistical unit. Fitted using a logistic model, it reveals a  
353 nonlinear saturation relationship between salinity and average burrow diameter characterized by  
354 'rapid growth at low salinity and stabilization at high salinity'. Under low to medium salinity (0.28–3.97  
355 PSU), the average burrow diameter increases with rising salinity, which is consistent with consistent  
356 with previous studies (Gingras et al., 2008, 2024). When salinity exceeds 18 PSU (e.g. at station 45), the  
357 diameter tends to stabilize, indicating that the *Perinereis* have reached their physiological tolerance  
358 limit for salinity (Feng et al., 2014). Regression analysis shows that the model has an  $R^2$  of 0.84, an  
359 adjusted  $R^2$  of 0.59, an  $F$ -value for analysis of variance of 24.69 and a  $P$ -value of 0.0391 (less than 0.05),  
360 indicating that the model is significantly effective overall.



361  
362 **Figure 9** – Relationship between burrow diameter (cm) and salinity (PSU) at sampling stations where  
363 *Perinereis* was present. (A) Scatter plot of the diameters of multiple burrows at *Perinereis* sampling  
364 stations under different salinity values. (B) Linear regression showing the relationship between salinity  
365 and average burrow diameter.

366 The characteristics of tidal flat bioturbation are collectively regulated by sediment grain size,  
367 turbidity and total organic carbon (TOC) (Li et al., 2019; Grandjean et al., 2024; Nauta et al., 2024). High  
368 turbidity is often accompanied by high sedimentation rates, and easily deposited flocculants can clog  
369 the filter-feeding organs of *Perinereis*, significantly affecting them. At the same time, reduced  
370 transparency inhibits phytoplankton photosynthesis, resulting in a decline in primary productivity  
371 (Cloern, 1987; Davies-Colley and Smith, 2001). The total organic carbon (TOC) content of a  
372 sedimentary environment can be used to characterize its nutritional status, food availability,  
373 environmental stability, and habitat suitability (Hyland et al., 2005; Li et al., 2016). Although there is a  
374 certain correlation between TOC and food sources, it is neither absolute nor precise, and can only be  
375 used as a basis for identifying potential food sources. Total organic carbon (TOC) includes both easily  
376 decomposable and refractory components, and the total amount of TOC does not directly reflect the

377 amount of active organic carbon available to infauna. This study demonstrates that it is only the easily  
378 decomposable components of TOC that serve as effective carbon and food sources for *Perinereis* (Li et  
379 al., 2022; Wang et al., 2024). Analysis of six *Perinereis* distribution stations in the intertidal zone of the  
380 Pearl River Delta (PRD) showed no significant correlation between physicochemical factors and  
381 bioturbation intensity. This differs from the traditional view of 'multi-factor synergistic regulation'.  
382 However, this conclusion is limited by the regional sedimentary environment and sample size, and is  
383 therefore mainly applicable to the study area. Spearman rank correlation analysis using Origin  
384 software ( $N = 6$ ) revealed that only mean grain size was strongly negatively correlated with  
385 bioturbation rate ( $r_s = -0.74$ ,  $P = 0.09$ ). While this did not reach the significant level of  $P < 0.05$ ,  $P < 0.1$   
386 indicates that the bioturbation rate decreases with increasing mean grain size. There were extremely  
387 weak correlations between the bioturbation rate and TOC ( $r_s = 0.20$ ,  $P = 0.70$ ), turbidity ( $r_s = 0.37$ ,  $P = 0.47$ )  
388 and salinity ( $r_s = 0.37$ ,  $P = 0.47$ ), and these were not statistically significant. Overall, mean grain size is the  
389 environmental factor with the strongest correlation, while the regulatory effect of other factors is  
390 insignificant (Figs. 10A–D). This may be related to infaunal dependence on sediment physical  
391 characteristics. Fine-grained sediments facilitate drilling and the stability of dwelling tubes, which can  
392 increase the intensity of sediment bioturbation. Meanwhile, the loose structure of coarse-grained  
393 sediments is not conducive to burrow maintenance, leading to a decrease in bioturbation rates (Ho et  
394 al., 1997). Therefore, mean grain size is the main factor affecting disruption behavior, with the roles of  
395 TOC, turbidity and salinity being relatively indirect or offset by flexible feeding strategies (Dorgan et  
396 al., 2008).



397

398 **Figure 10** – Relationship between TOC content (A), mean grain size (B), turbidity (C), salinity (D), and  
399 sediment disruption at stations where *Perinereis* was present in the Pearl River Delta tidal flats. Red  
400 stars denote sediment disruption at stations where *Perinereis* was present.

401 As typical biogenic traces, the burrows of the polychaete *Perinereis* preserve behavioral  
402 responses to environmental conditions (Kulkarni and Panchang, 2015) Burrow density is sensitive to  
403 population dynamics and short-term catastrophic events; a sudden decrease may indicate population  
404 collapse caused by anoxia, toxic pulses, or rapid sediment burial (Bromley and Ekdale, 1984;  
405 Dworschak and Rodrigues, 1997; Martin, 2004). Burrow diameter reflects individual physiological and  
406 behavioral adjustments and may indicate chronic, sublethal environmental stressors (Rodríguez-Tovar  
407 et al., 2014; Blankson et al., 2017; Koo and Seo, 2017; Tian et al., 2019).

408

## 409 **CONCLUSION**

410 This study examined the burrow systems of *Perinereis* in the intertidal zones of the Pearl River  
411 Delta (PRD), China. The results suggest that the benthic burrows of *Perinereis* exhibit a wide range of  
412 morphologies, including simple cylindrical, Y-shaped, U-shaped, and complex reticulated structures,  
413 which may exhibit local swellings at branch points. This morphological variation reflects the  
414 organism's ability to flexibly adjust its behavioral patterns in response to local microenvironmental  
415 conditions. Salinity was identified as the environmental factor significantly correlated with burrow  
416 diameter, with a nonlinear, saturating relationship: low to moderate salinity promotes burrow

Ocean and Coastal Research, 2026, v74 (in press)

417 enlargement, whereas burrow diameter tends to stabilize at high salinity levels approaching the  
418 species' physiological tolerance limit. However, salinity had no significant effect on burrow density.

419 Neither burrow diameter nor sediment bioturbation showed a significant correlation with single  
420 factors such as sediment grain size, salinity, turbidity, or total organic carbon (TOC) content. This  
421 suggests that these parameters are jointly regulated by biotic interactions and multiple environmental  
422 factors. The bioturbation rate was strongly negatively correlated with mean grain size, indicating that  
423 mean grain size is the primary factor controlling *Perinereis* bioturbation behavior. The influences of  
424 TOC, turbidity and salinity are relatively indirect, or may be offset by the infaunal flexible feeding  
425 strategies.

426 In terms of potential paleoenvironmental implications, the morphology of *Perinereis* burrows  
427 may indicate low-energy, nutrient-rich microenvironments in ancient intertidal zones. Differential  
428 responses in burrow density and diameter may reflect population dynamics and long-term  
429 environmental stress in paleo-ecosystems, which may offer preliminary insights for future  
430 paleoenvironmental reconstruction studies.

431

## 432 AI USE DISCLOSURE

433 During manuscript compilation, AI resources were only utilized to refine English diction and  
434 enhance overall manuscript legibility. All research conceptualization, original text composition,  
435 experimental design and statistical data analysis were accomplished independently by the author  
436 team; every figure and table was self-generated, with no artificial intelligence adopted for graph  
437 drafting or computational processing.

## 438 DATA AVAILABILITY STATEMENT

439 The authors confirm that all relevant data utilized in the research described herein are  
440 included within the article.

## 441 FUNDING

442 This research was supported by the National Natural Science Foundation of China (Grant No.  
443 42172130) and the Youth Backbone Teacher Training Program of Henan Provincial Universities  
444 (Grant No. 2023GGJS055).

445

## 446 AUTHOR CONTRIBUTION

447 Y.Y.W.: Conceptualization; Investigation; Data curation; Formal analysis; Visualization; Writing –  
448 Original draft preparation.

449 Z.Z.: Methodology; Formal analysis; Data curation; Validation; Writing – Reviewing and Editing.

450 M.M.: Investigation; Data curation; Methodology; Validation.

451 Y.M.Z.: Supervision; Methodology; Data curation; Validation; Writing – Reviewing and Editing.

452 G.C.Z.: Supervision; Project administration; Writing – Reviewing and Editing.

453 All authors: Approved the final version of the manuscript.

## 454 CONFLICTS OF INTEREST

455 We declare that we have no financial or personal relationships with other people or  
456 organizations that could inappropriately influence our work. There are no professional or other  
457 personal interests of any nature.

458

## 459 ACKNOWLEDGEMENTS

460 We thank Dr. Rubens Lopes, Editor-in-Chief of Ocean and Coastal Research, the anonymous  
461 Associate Editor, and two anonymous reviewers for their valuable and constructive comments over  
462 the past year, which were essential to the completion of this manuscript. We also acknowledge Dr.  
463 Chen Jie for CT scanning technical support in laboratory at Nanjing Institute of Soil Research, Chinese  
464 Academy of Sciences, and Dr. Yin Zongjun and Ms. Wu Suping for three-dimensional visualization in  
465 laboratory at Nanjing Institute of Geology and Paleontology, Chinese Academy of Sciences.

466

## 467 REFERENCES

- 468 Adikaram, M., Pitawala, A., Ishiga, H., Jayawardhana, D., 2017. Paleoenvironmental Reconstruction of  
469 Quaternary Sedimentation in Eastern Sri Lanka: An Ichnological Study. *Journal Geological Society Of*  
470 *India*, 89, 71-76. <https://doi.org/10.1007/s12594-017-0560-8>.
- 471 Alvarez, M.F., Bazterrica, M.C., Fanjul, E., Addino, M.S., Valiñas, M.S., Iribarne, O.O., Botto, F., 2018. Effects  
472 of two estuarine intertidal polychaetes on infaunal assemblages and organic matter under contrasting  
473 crab bioturbation activity. *Journal of Sea Research*, 139, 33-40.  
474 <https://doi.org/10.1016/j.seares.2018.06.008>
- 475 Ayranci, K., Dashtgard, S.E., MacEachern, J.A., 2014. A quantitative assessment of the neoichnology and  
476 biology of a delta front and prodelta, and implications for delta ichnology. *Palaeogeography,*  
477 *Palaeoclimatology, Palaeoecology*, 409, 114-134. <https://doi.org/10.1016/j.palaeo.2014.05.013>
- 478 Ayranci, K., Dashtgard, S.E., Walsh, J.P., 2013. Infaunal holothurian distributions and their traces in the Fraser  
479 River delta front and prodelta, British Columbia, Canada. *Palaeogeography, Palaeoclimatology,*  
480 *Palaeoecology*, 392, 232-246. <https://doi.org/10.1016/j.palaeo.2013.09.021>
- 481 Ayranci, K., Dashtgard, S.E., Walsh, J.P., 2016. Asymmetrical deltas below wave base: Insights from the Fraser  
482 River Delta, Canada. *Sedimentology*, 63(3), 761-779. <https://doi.org/10.1111/sed.12237>
- 483 Benkhedda, A., Defaflija, N., Cherif, A., Naimi, M.N., Mazouz, E.-H., Palma-Ramírez, A., 2021. Shallow  
484 marine trace fossils from the Middle Miocene of the Tebessa Basin (NE Algeria) and their  
485 palaeoenvironmental implications. *Revista Brasileira de Paleontologia*, 24(4), 323-335.  
486 <https://doi.org/10.1007/BF02990166>.
- 487 Bertrand, S., Daga, R., Bedert, R., Fontijn, K., 2014. Deposition of the 2011-2012 Cordon Caulle tephra (Chile,  
488 40°S) in lake sediments: Implications for tephrochronology and volcanology. *Journal of Geophysical*  
489 *Research: Earth Surface*, 119(12), 2555-2573. <https://doi.org/10.1002/2014jf003321>

- 490 Blankson, E.R., Adhikary, N.R.D., Klerks, P.L., 2017. The effect of lead contamination on bioturbation by  
491 *Lumbriculus variegatus* in a freshwater microcosm. *Chemosphere*, 167, 19-27.  
492 <https://doi.org/10.1016/j.chemosphere.2016.09.128>.
- 493 Bromley, R.G., Ekdale, A.A., 1984. Chondrites: A Trace Fossil Indicator of Anoxia in Sediments. *Science*,  
494 224(4651), 872-874. <https://doi.org/10.1126/science.224.4651.872>
- 495 Brown, D., Corlett, H., Kibblewhite, T., Whitaker, F., Zonneveld, J.-P., Gingras, M., 2024. Neoichnology of a  
496 Microtidal Carbonate Intertidal Zone: Abu Dhabi, UAE. *Palaios*, 39(9), 344-361.  
497 <https://doi.org/10.2110/palo.2023.042>.
- 498 Buatois, L.A., Mángano, M.G. 2011. *Ichnology: Organism-substrate interactions in space and time*. Cambridge  
499 University Press.
- 500 Buatois, L.A., Mángano, M.G., Pattison, S.A.J., 2019. Ichnology of prodeltaic hyperpycnite–turbidite channel  
501 complexes and lobes from the Upper Cretaceous Prairie Canyon Member of the Mancos Shale, Book  
502 Cliffs, Utah, USA. *Sedimentology*, 66(5), 1825-1860. <https://doi.org/10.1111/sed.12560>
- 503 Buatois, L.A., Santiago, N., Herrera, M., Plink-BjÖRklund, P., Steel, R.O.N., Espin, M., Parra, K., 2012.  
504 Sedimentological and ichnological signatures of changes in wave, river and tidal influence along a  
505 Neogene tropical deltaic shoreline. *Sedimentology*, 59(5), 1568-1612.  
506 <https://doi.org/10.1111/j.1365-3091.2011.01317.x>
- 507 Chen, Y., Deng, B., Saito, Y., Wang, Z., Yang, X., Wu, J., 2023. Pearl River sediment dispersal over its  
508 associated delta–estuary–shelf system during the Holocene. *Sedimentology*, 70(7), 2331-2354.  
509 <https://doi.org/10.1111/sed.13123>
- 510 Cloern, J.E., 1987. Turbidity as a control on phytoplankton biomass and productivity in estuaries. *Continental  
511 Shelf Research*, 7(11-12), 1367-1381. [https://doi.org/10.1016/0278-4343\(87\)90042-2](https://doi.org/10.1016/0278-4343(87)90042-2)
- 512 Cournane, S., León Vintó, L., Mitchell, P.I., 2010. Modelling the reworking effects of bioturbation on the  
513 incorporation of radionuclides into the sediment column: implications for the fate of particle-reactive  
514 radionuclides in Irish Sea sediments. *Journal of Environmental Radioactivity*, 101(11), 985-991.  
515 <https://doi.org/10.1016/j.jenvrad.2010.07.006>
- 516 Dashtgard, S.E., 2011a. Linking invertebrate burrow distributions (neoichnology) to physicochemical stresses  
517 on a sandy tidal flat: implications for the rock record. *Sedimentology*, 58(6), 1303-1325.  
518 <https://doi.org/10.1111/j.1365-3091.2010.01210.x>.
- 519 Dashtgard, S.E., 2011b. Neoichnology of the lower delta plain: Fraser River Delta, British Columbia, Canada:  
520 Implications for the ichnology of deltas. *Palaeogeography Palaeoclimatology Palaeoecology*, 307(1-4),  
521 98-108. <https://doi.org/10.1016/j.palaeo.2011.05.001>.
- 522 Davies-Colley, R., Smith, D., 2001. Turbidity suspended sediment, and water clarity: a review 1. *JAWRA  
523 Journal of the American Water Resources Association*, 37(5), 1085-1101.  
524 <https://doi.org/10.1111/j.1752-1688.2001.tb03624.x>.
- 525 Demircan, H., Uchman, A., 2016. Ichnology of prodelta deposits of the Mezardere Formation (late  
526 Eocene–early Oligocene) in the Gökçeada island, western Turkey. *Geodinamica Acta*, 28(1-2), 86-100.
- 527 Dorgan, K.M., Arwade, S.R., Jumars, P.A., 2008. Worms as wedges: Effects of sediment mechanics on  
528 burrowing behavior. *Journal of Marine Research*. <https://doi.org/10.1357/002224008785837130>
- 529 Dworschak, P.C., Rodrigues, S.D.A., 1997. A modern analogue for the trace fossil *Gyrolithes*: burrows of the  
530 thalassinidean shrimp *Axianassa australis*. *Lethaia*, 30(1), 41-52.  
531 <https://doi.org/10.1111/j.1502-3931.1997.tb00443.x>.
- 532 Fang, J., Jiang, Z., Fang, J., Kang, B., Gao, Y., Du, M., 2018. Selectivity of *Perinereis aibuhitensis* (Polychaeta,  
533 Nereididae) feeding on sediment. *Marine Biology Research*, 14(5), 478-483.  
534 <https://doi.org/10.1080/17451000.2018.1426864>

- 535 Feng, S., Huang, G., Lai, Z., Liang, W., Wu, M., Tang, L., Pan, Y., 2014. Tolerance studies on the temperature,  
536 salinity and desiccation in *Perinereis aibuhitensis*. *Transactions of Oceanology and Limnology*, 1,  
537 109-114.
- 538 Feng, X., Zhang, W., Zhu, Z., Chevuturi, A., Chen, W., 2021. Variability and changes in Pearl River Delta water  
539 level: Oceanic and atmospheric forcing perspectives. *Journal of Hydrometeorology*, 22(9), 2407-2422.  
540 <https://doi.org/10.1175/JHM-D-21-0037.1>.
- 541 Francoeur, A.A., Dorgan, K.M., 2014. Burrowing Behavior in Mud and Sand of Morphologically Divergent  
542 Polychaete Species (Annelida: Orbiniidae). *The Biological Bulletin*, 226(2), 131-145.  
543 <https://doi.org/10.1086/bblv226n2p131>
- 544 Freitas, R., Pires, A., Velez, C., Almeida, Â., Wrona, F.J., Soares, A.M.V.M., Figueira, E., 2015. The effects of  
545 salinity changes on the Polychaete *Diopatra neapolitana*: Impacts on regenerative capacity and  
546 biochemical markers. *Aquatic Toxicology*, 163, 167-176. <https://doi.org/10.1016/j.aquatox.2015.04.006>
- 547 Gingras, M.K., Dashtgard, S.E., MacEachern, J.A., Pemberton, S.G., 2008. Biology of shallow marine  
548 ichnology: a modern perspective. *Aquatic Biology*, 2, 255-268. <https://doi.org/10.3354/ab00055>
- 549 Gingras, M.K., MacEachern, J.A., Dashtgard, S.E., 2011. Process ichnology and the elucidation of  
550 physico-chemical stress. *Sedimentary Geology*, 237(3-4), 115-134.  
551 <https://doi.org/10.1016/j.sedgeo.2011.02.006>
- 552 Gingras, M.K., MacEachern, J.A., Dashtgard, S.E., Bann, K.L., 2024. The Teichichnus Ichnofacies: Its  
553 neoichnological basis and identification in the rock record. *Sedimentology*, 72(2), 408-441.  
554 <https://doi.org/10.1111/sed.13246>
- 555 Grandjean, T.J., Weenink, R., van der Wal, D., Addink, E.A., Hu, Z., Liu, S., Wang, Z.B., Yuan, L., Bouma,  
556 T.J., 2024. Critical turbidity thresholds for maintenance of estuarine tidal flats worldwide. *Nature*  
557 *Geoscience*, 17(6), 539-544. <https://doi.org/10.1038/s41561-024-01431-3>
- 558 Hale, R., Boardman, R., Mavrogordato, M.N., Sinclair, I., Tolhurst, T.J., Solan, M., 2015. High-resolution  
559 computed tomography reconstructions of invertebrate burrow systems. *Scientific Data*, 2(1), 1-5.  
560 <https://doi.org/10.1038/sdata.2015.52>
- 561 Herringshaw, L.G., Sherwood, O.A., McIlroy, D., 2010. Ecosystem Engineering by Bioturbating Polychaetes in  
562 Event Bed Microcosms. *Palaios*, 25(1), 46-58. <https://doi.org/10.2110/palo.2009.p09-055r>
- 563 Ho, K.K., Kyoo, Y.S., Jin, C.Y., 1997. Sediment preference and burrow shape of the polychaete, *Perinereis*  
564 *aibuhitensis* according to the laboratory culture. *Korean Journal of Fisheries and Aquatic Sciences*,  
565 30(4), 634-639.
- 566 Howman, R.M., Mavrogordato, M.N., Alvarez-Borges, F., Solan, M., 2024. Computed tomography  
567 reconstructions of burrow networks for the Opheliid polychaete, *Armandia cirrhosa*. *Scientific Data*,  
568 11(1), 695. <https://doi.org/10.1038/s41597-024-03557-w>
- 569 Hyland, J., Balthis, L., Karakassis, I., Magni, P., Petrov, A., Shine, J., Vestergaard, O., Warwick, R., 2005.  
570 Organic carbon content of sediments as an indicator of stress in the marine benthos. *Marine Ecology*  
571 *Progress Series*, 295, 91-103. <https://doi.org/10.3354/meps295091>
- 572 Jia, P., Xia, Z., Yin, Y., Xue, Q., 2016. Lingdingyang Bay, Pearl River Estuary (China): geomorphological  
573 evolution and hydrodynamics. *Geological Society, London, Special Publications*, 429, 171-184.  
574 <https://doi.org/10.1144/SP429.14>
- 575 Knaust, D., Bromley, R.G. 2012. *Trace fossils as indicators of sedimentary environments* (Vol. 64). Newnes.
- 576 Koo, B.J., Seo, J., 2017. Sediment reworking by a polychaete, *Perinereis aibuhitensis*, in the intertidal  
577 sediments of the Gomso Bay, Korea. *Ocean Science Journal*, 52(4), 511-518.  
578 <https://doi.org/10.1007/s12601-017-0037-0>
- 579 Kruger, C.D., Woodin, S.A., 1993. Spatial persistence and sediment disturbance of an arenicolid polychaete.  
580 *Limnology and Oceanography*, 38(3), 509-520. <https://doi.org/10.4319/lo.1993.38.3.0509>

- 581 Kulkarni, K.G., Panchang, R., 2015. New Insights into Polychaete Traces and Fecal Pellets: Another Complex  
582 Ichnotaxon? *PLOS One*, 10(e0139933). <https://doi.org/10.1371/journal.pone.0139933>.
- 583 Kumar, A., 2017. Recent biogenic traces from the coastal environments of the southern Red Sea coast of Saudi  
584 Arabia. *Arabian Journal of Geosciences*, 10(22), 500. <https://doi.org/10.1007/s12517-017-3293-5>
- 585 La Croix, A.D., Dashtgard, S.E., Gingras, M.K., Hauck, T.E., MacEachern, J.A., 2015. Bioturbation trends  
586 across the freshwater to brackish-water transition in rivers. *Palaeogeography, Palaeoclimatology,*  
587 *Palaeoecology*, 440, 66-77. <https://doi.org/10.1016/j.palaeo.2015.08.030>
- 588 Li, D., Liu, X., Liu, Z., Zhao, X., 2016. Variations in total organic carbon and acid-volatile sulfide distribution  
589 in surface sediments from Luan River Estuary, China. *Environmental Earth Sciences*, 75(14), 1073.  
590 <https://doi.org/10.1007/s12665-016-5873-1>.
- 591 Li, J., Hu, R., Guo, Y., Chen, S., Xie, X., Qin, J.G., Ma, Z., Zhu, C., Pei, S., 2019. Bioturbation of peanut  
592 worms *Sipunculus nudus* on the composition of prokaryotic communities in a tidal flat as revealed by  
593 16S rRNA gene sequences. *MicrobiologyOpen*, 8(8), e00802. <https://doi.org/10.1002/mbo3.802>
- 594 Li, J., Shi, X., Chen, Y.D., Zhang, L., 2020. Proposing a trend-based time-varying approach to assess climate-  
595 and human-induced impacts on streamflow. *Hydrological Sciences Journal*, 65(12), 2043-2056.  
596 <https://doi.org/10.1080/02626667.2020.1785625>
- 597 Li, L., Dai, M., Zhao, Y.-c., Chen, Y.-s., Xu, C.-l., Wang, S.-j., Jiang, M., 2022. Study on integrated  
598 bioremediation of *Suaeda glauca* and *Perinereis aiuhitensis* on *Meretrix meretrix* aquaculture ponds.
- 599 Li, Z., Wang, X., Vandenbergh, J., Lu, H., 2021. Extension of the Upper Yellow River into the Tibet Plateau:  
600 Review and New Data. *Quaternary*, 4(2), 14. <https://doi.org/10.3390/quat4020014>
- 601 Liu, F., Yuan, L., Yang, Q., Ou, S., Xie, L., Cui, X., 2014. Hydrological responses to the combined influence of  
602 diverse human activities in the Pearl River delta, China. *Catena*, 113, 41-55.  
603 <https://doi.org/10.1016/j.catena.2013.09.003>.
- 604 Martin, K.D., 2004. A re-evaluation of the relationship between trace fossils and dysoxia. *Geological Society,*  
605 *London, Special Publications*, 228(1), 141-156. <https://doi.org/10.1144/GSL.SP.2004.228.01.08>.
- 606 Mazik, K., Curtis, N., Fagan, M.J., Taft, S., Elliott, M., 2008. Accurate quantification of the influence of  
607 benthic macro- and meio-fauna on the geometric properties of estuarine muds by micro computer  
608 tomography. *Journal of Experimental Marine Biology and Ecology*, 354(2), 192-201.  
609 <https://doi.org/10.1016/j.jembe.2007.11.006>
- 610 Mimier, D., Żbikowski, J., 2017. Effect of substrate change on macrozoobenthos structure. *Ecological*  
611 *Questions*, 27, 109-118. <https://doi.org/10.12775/eq.2017.032>
- 612 Morelle, J., Huguet, A., Richard, A., Laverman, A.M., Roose-Amsaleg, C., Parlanti, E., Sourzac, M., Mesnage,  
613 V., Lecoq, N., Deloffre, J., Viollier, E., Maire, O., Orvain, F., 2024. Antagonistic impacts of benthic  
614 bioturbator species: Interconnected effects on sedimentary properties, biogeochemical variables, and  
615 microbial dynamics. *Journal of Experimental Marine Biology and Ecology*, 573, 152000.  
616 <https://doi.org/10.1016/j.jembe.2024.152000>
- 617 Moyano Paz, D., Richiano, S., Varela, A.N., Gómez Dacál, A.R., Poiré, D.G., 2020. Ichnological signatures  
618 from wave- and fluvial-dominated deltas: The LA Anita formation, upper Cretaceous,  
619 austral-magallanes basin, Patagonia. *Marine and Petroleum Geology*, 114, 104168.  
620 <https://doi.org/10.1016/j.marpetgeo.2019.104168>
- 621 Nauta, J., Leurs, G., Nieuwenhuis, B.O., Mathijssen, D.R.A.H., Olf, H., Bouma, T.J., van der Wal, D., Hijner,  
622 N., Regalla, A., Pontes, S.L., Govers, L.L., 2024. Bioturbation by Benthic Stingrays Alters the  
623 Biogeomorphology of Tidal Flats. *Ecosystems*, 27(4), 493-507.  
624 <https://doi.org/10.1007/s10021-024-00901-4>
- 625 Nel, R., McLachlan, A., Winter, D.P.E., 2001. The effect of grain size on the burrowing of two *Donax* species.  
626 *Journal of Experimental Marine Biology and Ecology*, 265(2), 219-238.  
627 [https://doi.org/10.1016/s0022-0981\(01\)00335-5](https://doi.org/10.1016/s0022-0981(01)00335-5)

- 628 Olabarria, C., Urgorri, V., Troncoso, J.S., 1998. The influence of physicochemical parameters on the  
629 distribution of dominant bivalve species in the ensenada do Baño (Ria de Ferrol) in Northwest of Spain.  
630 *13*(3), 81-93.
- 631 Palomo, G., Iribarne, O., 2000. Sediment bioturbation by polychaete feeding may promote sediment stability.  
632 *Bulletin of Marine Science*, 67(1), 249-257. <https://doi.org/10.1515/BOT.2000.041>.
- 633 Palomo, G., Martinetto, P., Iribarne, O., 2004. Changes in the feeding behavior of the deposit-feeding  
634 polychaete *Laeonereis acuta* on soft sediments inhabited by burrowing crabs. *Marine Biology*, 145(4),  
635 657-667. <https://doi.org/10.1007/s00227-004-1352-4>.
- 636 Pang, M., Xu, R., Zhu, T., Wang, C., Kaisam, J.P., 2021. Water quality improvement measures at the Yagang  
637 cross-section in the Pearl River Delta based on the calculation of excessive pollutant fluxes. *Water*  
638 *Supply*, 21(4), 1778-1792. <https://doi.org/10.2166/ws.2020.345>
- 639 Passarelli, C., Olivier, F., Paterson, D.M., Hubas, C., 2012. Impacts of biogenic structures on benthic  
640 assemblages: microbes, meiofauna, macrofauna and related ecosystem functions. *Marine Ecology*  
641 *Progress Series*, 465(6), 85-97. <https://doi.org/10.3354/meps09915>
- 642 Passarelli, C., Olivier, F., Paterson, D.M., Meziane, T., Hubas, C., 2014. Organisms as cooperative ecosystem  
643 engineers in intertidal flats. *Journal of Sea Research*, 92, 92-101.  
644 <https://doi.org/10.1016/j.seares.2013.07.010>
- 645 Patel, S.J., Desai, B.G., 2009. Animal-sediment relationship of the crustaceans and polychaetes in the intertidal  
646 zone around Mandvi, Gulf of Kachchh, Western India. *Journal of the Geological Society of India*, 74(2),  
647 233-259. <https://doi.org/10.1007/s12594-009-0125-6>
- 648 Pennafirme, S., Machado, A.S., Machado, A.C., Lopes, R.T., Lima, I.C.B., Crapez, M.A.C., 2019. Monitoring  
649 bioturbation by a small marine polychaete using microcomputed tomography. *Micron*, 121, 77-83.  
650 <https://doi.org/10.1016/j.micron.2019.03.004>
- 651 Petrash, D.A., Lalonde, S.V., Gingras, M.K., Konhauser, K.O., 2011. A surrogate approach to studying the  
652 chemical reactivity of burrow mucous linings in marine sediments. *Palaios*, 26(9), 594-600.  
653 <https://doi.org/10.2110/palo.2010.p10-140r>.
- 654 Rodríguez-Tovar, F.J., Nagy, J., Reolid, M., 2014. Palaeoenvironment of Eocene prodelta in Spitsbergen  
655 recorded by the trace fossil *Phycosiphon incertum*. *Polar Research*, 33(1), 23786.  
656 <https://doi.org/10.3402/polar.v33.23786>
- 657 Rowshan, O., Sakhaei, N., Zolgharnein, H., Paknezhad, H., Taheri, M., 2023. Research Article: Spatial  
658 distribution and structure of benthic polychaete communities in shallow waters of the south Caspian  
659 Sea, Iran. *Iranian Journal of Fisheries Sciences*, 22(1), 44-65. <https://doi.org/10.22092/ijfs.2023.128618>
- 660 Sendra, J., Reolid, M., Reolid, J., 2019. Palaeoenvironmental interpretation of the Pliocene fan-delta system of  
661 the Vera Basin (SE Spain): Fossil assemblages, ichnology and taphonomy. *Palaeoworld*, 29(4),  
662 769-788. <https://doi.org/10.1016/j.palwor.2019.11.001>
- 663 Shetty, A., Goyal, A., 2022. Total organic carbon analysis in water – A review of current methods. *Materials*  
664 *Today Proceedings*, 65(8), 3881-3886. <https://doi.org/10.1016/j.matpr.2022.07.173>
- 665 Song, W., Li, Y., 2023. Tidal flat microbial communities between the Huaihe estuary and Yangtze River estuary.  
666 *Environmental Research*, 238(1), 117141. <https://doi.org/10.1016/j.envres.2023.117141>
- 667 Sun, T., Liu, C.e., Li, X., An, D., Yu, H., Ma, Z., Liu, F., 2019. The effect of substrate grain size on burrowing  
668 ability and distribution characteristics of *Perinereis aibuhitensis*. *Acta Oceanologica Sinica*, 38(12),  
669 52-58. <https://doi.org/10.1007/s13131-019-1348-z>
- 670 Tian, S., Tong, Y., Hou, Y., 2019. The effect of bioturbation by polychaete *Perinereis aibuhitensis* on release  
671 and distribution of buried hydrocarbon pollutants in coastal muddy sediment. *Marine Pollution Bulletin*,  
672 149, 110487. <https://doi.org/10.1016/j.marpolbul.2019.110487>

- 673 Virtasalo, J.J., Leipe, T., Moros, M., Kotilainen, A.T., 2011. Physicochemical and biological influences on  
674 sedimentary-fabric formation in a salinity and oxygen-restricted semi-enclosed sea: Gotland Deep,  
675 Baltic Sea. *Sedimentology*, 58(2), 352-375. <https://doi.org/10.1111/j.1365-3091.2010.01166.x>
- 676 Wang, Y.Y., Gou, S.L., Wang, C., Zhang, G.c., Uchman, A., Wetzel, A., 2024. The crab *Macrophthalmus*  
677 *japonicus* burrows on a tidal flat of the Yellow River Delta in China: Their 3D morphological variability  
678 in relation to physicochemical conditions and palaeoichnological perspective. *Palaeogeography,*  
679 *Palaeoclimatology, Palaeoecology*, 638, 112037. <https://doi.org/10.1016/j.palaeo.2024.112037>
- 680 Wang, Y.Y., Wang, X.Q., Uchman, A., Hu, B., Song, H.b., 2019. Burrows of the polychaete *Perinereis*  
681 *aibuhiutensis* on a tidal flat of the yellow river delta in China: implications for the ichnofossils  
682 *Polykladichnus* and *Archaeonassa*. *Palaios*, 34(5), 271-279. <https://doi.org/10.2110/palo.2018.105>.
- 683 Wang, Y.Y., Zhang, Y.B., Gou, S.L., Zhang, G.C., 2025. 3D morphology of crab (*Macrophthalmus japonicus*)  
684 burrows from the Pearl River Delta front, China: The physicochemical factors, with implications for the  
685 rock record. *Journal of Palaeogeography*, 14(1), 203-220. <https://doi.org/10.1016/j.jop.2024.09.004>
- 686 Wei, Z., Huang, S., Xu, J., Yuan, C., Zhang, M., Wang, C., 2024. Geochemical evolution of geothermal waters  
687 in the Pearl River Delta region, South China: Insights from water chemistry and isotope geochemistry.  
688 *Journal of Hydrology: Regional Studies*, 51, 101670. <https://doi.org/10.1016/j.ejrh.2024.101670>
- 689 Xiao, M., Cui, Y., 2021. Source of Evaporation for the Seasonal Precipitation in the Pearl River Delta, China.  
690 *Water Resources Research*, 57(8), eWR028564(028561-028512). <https://doi.org/10.1029/2020wr028564>
- 691 Yang, F., Ji, X., Zhang, W., Zou, H., Jiang, W., Xu, Y., 2022. Characteristics and driving mechanisms of salinity  
692 stratification during the wet season in the Pearl River Estuary, China. *Journal of Marine Science and*  
693 *Engineering*, 10(12), 1927. <https://doi.org/10.3390/jmse10121927>
- 694 Zhang, W., Cao, Y., Zhu, Y., Wu, Y., Ji, X., He, Y., Xu, Y., Wang, W., 2017. Flood frequency analysis for  
695 alterations of extreme maximum water levels in the Pearl River Delta. *Ocean Engineering*, 129,  
696 117-132. <https://doi.org/10.1016/j.oceaneng.2016.11.013>
- 697 Zhang, W., Ruan, X., Zheng, J., Zhu, Y., Wu, H., 2010. Long-term change in tidal dynamics and its cause in the  
698 Pearl River Delta, China. *Geomorphology*, 120(3-4), 209-223.  
699 <https://doi.org/10.1016/j.geomorph.2010.03.031>

700

701

This preprint was submitted under the following conditions:

- The authors declare that the necessary Terms of Free and Informed Consent of participants or patients in the research were obtained and are described in the manuscript, when applicable.
- The authors declare that the preparation of the manuscript followed the ethical norms of scientific communication.
- The authors declare that they are aware that they are solely responsible for the content of the preprint and that the deposit in SciELO Preprints does not mean any commitment on the part of SciELO, except its preservation and dissemination.
- The authors declare that the data, applications, and other content underlying the manuscript are referenced.
- The deposited manuscript is in PDF format.
- The authors declare that the research that originated the manuscript followed good ethical practices and that the necessary approvals from research ethics committees, when applicable, are described in the manuscript.
- The authors declare that once a manuscript is posted on the SciELO Preprints server, it can only be taken down on request to the SciELO Preprints server Editorial Secretariat, who will post a retraction notice in its place.
- The authors agree that the approved manuscript will be made available under a [Creative Commons CC-BY](#) license.
- The submitting author declares that the contributions of all authors and conflict of interest statement are included explicitly and in specific sections of the manuscript.
- The authors declare that the manuscript was not deposited and/or previously made available on another preprint server or published by a journal.
- If the manuscript is being reviewed or being prepared for publishing but not yet published by a journal, the authors declare that they have received authorization from the journal to make this deposit.
- The submitting author declares that all authors of the manuscript agree with the submission to SciELO Preprints.